crystals

MDPI

Article

Wavy Ice Patterns as a Result of Morphological Instability of an Ice–Water Interface with Allowance for the Convective–Conductive Heat Transfer Mechanism

Dmitri V. Alexandrov [1,*], Eugenya V. Makoveeva [1] and Alina D. Pashko [2]

[1] Laboratory of Multi-Scale Mathematical Modeling, Department of Theoretical and Mathematical Physics, Ural Federal University, Lenin Ave., 51, Ekaterinburg 620000, Russia; e.v.makoveeva@urfu.ru

[2] Institute of Natural Sciences and Mathematics, Ural Federal University, Lenin Ave., 51, Ekaterinburg 620000, Russia

* Correspondence: dmitri.alexandrov@urfu.ru

Abstract: In this research, the wavy ice patterns that form due to the evolution of morphological perturbations on the water–ice phase transition interface in the presence of a fluid flow are studied. The mathematical model of heat transport from a relatively warm fluid to a cold wall includes the mechanism of convective–conductive heat transfer in liquid and small sinusoidal perturbations of the water–ice interface. The analytical solutions describing the main state with a flat phase interface as well as its small morphological perturbations are derived. Namely, the migration velocity of perturbations and the dispersion relation are found. We show that the amplification rate of morphological perturbations changes its sign with variation of the wavenumber. This confirms the existence of two different crystallization regimes with (i) a stable (flat) interfacial boundary and (ii) a wavy interfacial boundary. The maximum of the amplification rate representing the most dangerous (quickly growing) perturbations is found. The theory is in agreement with experimental data.

Keywords: crystallization; water–ice interface; convection; heat transfer; wavy ice surface

Citation: Alexandrov, D.V.; Makoveeva, E.V.; Pashko, A.D. Wavy Ice Patterns as a Result of Morphological Instability of an Ice–Water Interface with Allowance for the Convective–Conductive Heat Transfer Mechanism. *Crystals* **2024**, *14*, 138. https://doi.org/10.3390/cryst14020138

Academic Editor: Catalin Popescu

Received: 19 December 2023
Revised: 24 January 2024
Accepted: 29 January 2024
Published: 30 January 2024

1. Introduction

A mathematical description of phase transformations in the presence of convection in liquid is a complex task with a moving boundary, the position of which is determined by solving the problem. In addition, such problems are strongly complicated by various peculiarities of the hydrodynamic flow near a phase transition boundary, leading to a mixed convective–conductive mechanism of heat and mass transfer. Examples of such events are the processes of water freezing in rivers, lakes, and seas, the solidification of molten metal in a mold and magma in a magmatic chamber, and the growth of stenoses in blood vessels leading to limited or complete cessation of blood flow (see, among others, [1–7]).

The nonlinearity of such a phase transformation problem arises for several reasons. Firstly, convective terms appear in the heat and mass transfer equations in the moving coordinate system connected with the growing/melting interfacial boundary [8–11]. This is due to the fact that the ordinary derivative with respect to time can be expanded into local and convective components. Secondly, nonlinearity may be initially involved in the boundary conditions at the moving crystallization front when the dependence of phase transformation temperature on impurity concentration, front curvature, and atomic kinetics is considered [12,13]. Thirdly, in the case of turbulent fluid flow, additional diffusion terms of turbulent heat and mass fluxes appear in the equations of heat and mass transfer [14–16]. The presence of such terms makes nonlinear the heat and mass transport in liquid due to the strong mixing of liquid and the occurrence of complex circulation currents near the interphase boundary [17]. Fourth, a nonlinearity of the problem arises due to the morphological instability of the phase transformation boundary and the formation of new periodic and/or irregular crystallization scenarios [18–24].

The presence of convection in liquid strongly affects the heat and mass transfer near a phase transformation boundary. For example, convection mixes the liquid phase and partially levels the temperature and concentration distributions. This, in particular, leads to the appearance of convective components in heat and mass fluxes at the liquid–solid interface. Thus, the heat and mass fluxes at this interface become of a mixed type (conductive–convective), i.e., they have both conductive and convective contributions [25–27]. Taking this fact into account, a complete mathematical model of the directional crystallization process of a binary liquid has recently been formulated with allowance for the conductive–convective heat and mass transfer mechanism [28]. In this paper, a linear analysis of the morphological instability of a flat crystallization front in the presence of convection was also carried out and a new criterion for constitutional supercooling origination was derived, which demonstrated the existence of four crystallization scenarios. The theory developed in [28] also showed a significant influence of convection on the crystallization process as a whole and on the stability criterion, which was thoroughly studied by various scientific groups after the classical theory by Mullins and Sekerka [18] was published. Below, we investigate the influence of convective heat transfer on the morphological stability of the liquid–solid interface, which leads to the appearance of so-called wavy ice layers (Figure 1) [29–34].

Figure 1. A wavy water–ice surface.

2. Morphological Stability

A wavy ice layer, as shown in Figure 1, results from the development of liquid–solid interface instability in the hydrodynamic flow [35]. At the initial moment of time $t = 0$, a groove was made on the ice surface (see Figure 8 in [35]), which transformed over time and led to the formation of the wavy ice surface. In the course of time, the downstream side of the groove melts to form a longer groove and the ice downstream of the groove becomes slightly wider. Approximately 2–3 h later, a second groove begins to form downstream about 15 cm from the initial groove. Over time, this sinusoidal-like wave propagates downstream, leading to the formation of several waves. As this takes place, the amplitudes of these waves also increase until the first wave downstream of the initial groove develops a sharp crest after about $t = 3$ h. Subsequent waves also develop sharp crests, after which further changes in wave amplitudes cease and a so-called wavy or ripple ice surface is formed (wave crests are placed in a perpendicular to the flow). The waves continue to migrate slowly downstream. In the fluid flow downstream of the crest of each wave, there is a region of separated flow. An important point is that the ice surface is stable if it is reverted to a planar liquid–solid surface some time after the groove has been made. On the other hand, in the case of instability, the initial groove leads to the formation of a wavy surface, as described above.

Let us formulate below a mathematical model of heat transfer describing the crystallization process with a wavy water–ice interface shown in Figure 2. The phase interface position $s_i(x,t) = s_0(t) + \eta(x,t)$ is considered to be a sum of two contributions: the growing ice layer s_0 and its perturbation $\eta(x,t)$ of the form

$$\eta(x,t) = A\sin[k(x-ct)]\exp(\alpha t), \quad (1)$$

where x and t are the spatial and time variables, respectively; A is the amplitude of perturbations; α and k are their amplification rate and wavenumber, respectively; and c is the migration velocity of the surface wave. Here, the water–ice interface perturbation is assumed to be small, i.e., $|\eta(x,t)| \ll s_0(t)$.

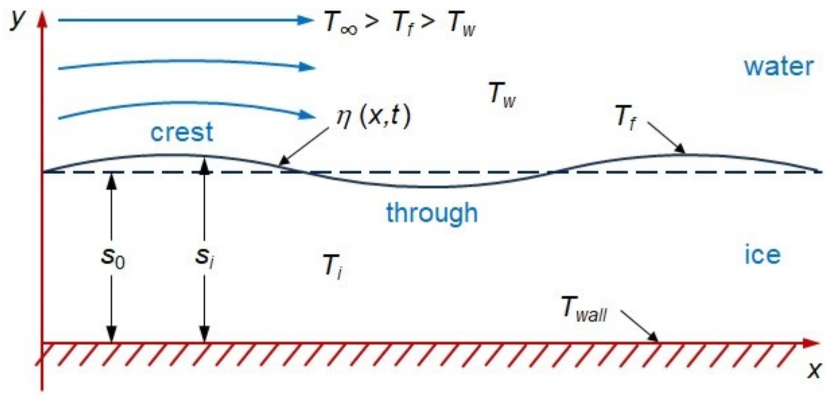

Figure 2. A scheme of crystallization process with a wavy water–ice surface.

At the interfacial boundary, fluid currents result in a conductive–convective heat flux at the fluid side [25–28]. In addition, the temperature continuity condition is fulfilled at this boundary. Taking this into account, we have the following heat balance and temperature continuity boundary conditions

$$\rho_i L \frac{\partial s_i}{\partial t} = k_i \frac{\partial T_i}{\partial y} - k_w \frac{\partial T_w}{\partial y} - h(T_\infty - T_w),\ y = s_i,$$
$$T_w = T_i = T_f,\ y = s_i. \tag{2}$$

Here, T_i and T_w are the temperatures of ice and water, respectively, k_i and k_w are their thermal conductivities, respectively, ρ_i is the density of ice, L is the latent heat parameter, h is the heat-transfer coefficient, T_∞ is the temperature in water far from the water–ice phase interface, and T_f is the temperature at the phase interface. Note that the simultaneous convective–conductive heat transfer flux at the boundary $y = s_i$ represents the main novelty of the model under consideration.

In the case of slow motion of the water–ice interface, the temperature profile of the ice is described by the stationary heat conduction equation [36,37]

$$\nabla^2 T_i = 0,\ 0 \le y \le s_i(x,t). \tag{3}$$

The temperature is fixed at the cold wall (bottom) $y = 0$, and we have the boundary condition

$$T_i = T_{wall},\ y = 0. \tag{4}$$

The temperature distribution in ice with a perturbed interfacial boundary $y = s_i(x,t)$ can be found using the perturbation method [38]. To do this, we represent the temperature in ice T_i as the sum of mean temperature T_{i0} and its perturbation T_{i1}, i.e.,

$$T_i(x,y,t) = T_{i0}(y) + T_{i1}(x,y,t),\ 0 \le y \le s_i(x,t). \tag{5}$$

In addition, we assume that [38] $|T_{i1}| \ll |T_0|$.

By expanding the second boundary condition (2) into a Taylor series on the perturbed boundary $y = s_i(x,t)$, restricting ourselves to the linear terms, and moving this boundary to the point $y = s_0$ assuming small perturbations $|\eta(x,t)| \ll s_0$, we obtain

$$T_{i0} + \frac{dT_{i0}}{dy}\eta + T_{i1} = T_f,\ y = s_0. \tag{6}$$

Now, equating the terms of the same order of magnitude in perturbations in (6) and considering expressions (3) and (4), we arrive at the following problems for the determination of temperature contributions T_{i0} and T_{i1}

$$\begin{aligned} \frac{d^2 T_{i0}}{dy^2} &= 0,\ 0 \le y \le s_0, \\ T_{i0} &= T_f,\ y = s_0, \\ T_{i0} &= T_{wall},\ y = 0 \end{aligned} \tag{7}$$

and

$$\begin{aligned} \nabla^2 T_{i1} &= 0,\ 0 \le y \le s_0, \\ T_{i1} &= -\frac{dT_{i0}}{dy}\eta,\ y = s_0, \\ T_{i1} &= 0,\ y = 0. \end{aligned} \tag{8}$$

Their solutions read as

$$T_{i0}(y) = T_{wall} + \frac{T_f - T_{wall}}{s_0} y \tag{9}$$

and

$$T_{i1}(x, y, t) = -(T_f - T_{wall}) \frac{\eta(x,t)}{s_0} \frac{\sinh(ky)}{\sinh(ks_0)}, \tag{10}$$

where $\eta(x,t)$ is given by expression (1). Distributions (9) and (10) determine the temperature field in ice accordingly to expression (5).

Note that the heat-transfer coefficient $h = h_0 + h_1$ should be treated as the sum of the constant main value $h_0 = \alpha_h \rho_w c_w u_*$ [39,40] and its perturbation h_1 of the form [35]

$$h_1(x,t) = f h_0 A^+ \sin[k(x - ct) + \phi] \exp(\alpha t), \tag{11}$$

where α_h is the convective heat transfer coefficient, ρ_w is the density of water, u_* is the friction velocity, f is the perturbation amplitude, $A^+ = Au_*/\nu_w$, ν_w is the kinematic viscosity of water, and ϕ is the phase shift between the heat transfer and water–ice interface perturbations.

Let us now perturb the boundary conditions (2) at the water–ice interface in accordance with the linear stability theory for small morphological perturbations [18,22,23]. Hence, assuming that the temperature in water represents the sum of a mean quantity T_{w0} and its perturbation T_{w1} ($|T_{w1}| \ll |T_{w0}|$)

$$T_w(x,y,t) = T_{w0}(y) + T_{w1}(x,y,t),\ y \ge s_i(x,t), \tag{12}$$

expanding the boundary conditions (2) into a Taylor series on the perturbed water–ice boundary $y = s_i(x,t)$ and moving this boundary to the point $y = s_0$, we obtain

$$\begin{aligned} \rho_i L\left(\frac{ds_0}{dt} + \frac{\partial \eta}{\partial t}\right) &= k_i \frac{dT_{i0}}{dy} + k_i \frac{d^2 T_{i0}}{dy^2}\eta + k_i \frac{\partial T_{i1}}{\partial y} - k_w \frac{dT_{w0}}{dy} \\ -k_w \frac{d^2 T_{w0}}{dy^2}\eta - k_w \frac{\partial T_{w1}}{\partial y} &- (h_0 + h_1)\left(T_\infty - T_{w0} - \frac{dT_{w0}}{dy}\eta - T_{w1}\right),\ y = s_0, \end{aligned} \tag{13}$$

$$T_{w1} + \frac{dT_{w0}}{dy}\eta = 0,\ y = s_0. \tag{14}$$

Here, $T_{w0} = T_f$ at $y = s_0$, temperatures T_{i0} and T_{i1} are given by distributions (9) and (10), respectively, and η and h_1 are defined by expressions (1) and (11), respectively.

Equating now the terms of the same order of smallness in perturbations in Equation (13), we obtain

$$\rho_i L \frac{ds_0}{dt} = k_i \frac{T_f - T_{wall}}{s_0} - k_w \left(\frac{dT_{w0}}{dy} \right)_{y=s_0} - h_0 \left(T_\infty - T_f \right). \tag{15}$$

$$\rho_i L \frac{\partial \eta}{\partial t} = -\frac{k_i (T_f - T_{wall}) k \eta}{s_0 \tanh(k s_0)} - k_w \frac{d^2 T_{w0}}{dy^2} \eta - k_w \frac{\partial T_{w1}}{\partial y} - h_1 (T_\infty - T_f), \; y = s_0. \tag{16}$$

Note that Formulas (10) and (14) were used when deriving expression (16).

Generally speaking, the temperature derivatives dT_{w0}/dy and d^2T_{w0}/dy^2 at $y = s_0$ can be the functions of s_0. Therefore, expression (15) supplemented with the initial condition $s_0(t) = s_0(0)$ at $t = 0$ represents the standard Cauchy problem for the determination of ice layer thickness $s_0(t)$. In the case of slow ice growth, s_0 is practically independent of time t and the left hand-side of Equation (15) can be omitted. In this case, expression (15) represents an algebraic equation defining the ice thickness s_0.

By substituting η and h_1 from (1) and (11) into (16) we conclude that $\partial T_{w1}/\partial y$ at $y = s_0$ should be a similar function of x and t, i.e.,

$$\left(\frac{\partial T_{w1}}{\partial y} \right)_{y=s_0} = g_w A^+ \sin[k(x - ct) + \psi] \exp(\alpha t), \tag{17}$$

where g_w and ψ stand for the perturbation amplitude and its phase shift.

Now combining (1), (11), (16), and (17), we find the migration velocity c and dispersion relation

$$c(k^+) = \frac{1}{\rho_i L k^+} \Big(h_0 (T_\infty - T_f) f \sin\phi + k_w g_w \sin\psi \Big), \tag{18}$$

$$\begin{aligned} \alpha(k^+) = &-\frac{h_0 (T_\infty - T_f) u_* k^+}{\rho_i L \nu_w} \left(\frac{f \cos\phi}{k^+} + \frac{k_i (T_f - T_{wall})}{h_0 s_0 (T_\infty - T_f) \tanh(k^+ u_* s_0 / \nu_w)} \right) \\ &- \frac{k_w}{\rho_i L} \left(\left(\frac{d^2 T_{w0}}{dy^2} \right)_{y=s_0} + \frac{g_w u_* \cos\psi}{\nu_w} \right), \end{aligned} \tag{19}$$

where $k^+ = k\nu_w/u_*$ is the dimensionless wavenumber. Here f, ϕ, g_w, and ψ can be the functions of k^+. Experiments [35] show that f and ϕ can be approximated by the following dependencies

$$f(k^+) = 50.44 (k^+)^{1.435}, \; \phi(k^+) = 13.08 + 4.32 \ln k^+ + 0.41 (\ln k^+)^2. \tag{20}$$

Note that expressions (19) and (20) derived with allowance for a mixed type of convective–conductive heat transfer in water represent the main result of our theory.

Let us especially highlight that the temperature field $T_{w0}(y)$ in liquid can be found from various models of heat transfer in a hydrodynamic flow [25–27,41,42]. In the case of a laminar flow, the temperature field is governed by the convective heat transfer equation. In the case of turbulent fluid flow, the turbulent heat flux must be taken into account in the heat transfer equation [14–16]. Another way to find the temperature distribution in liquid is to perform an experiment that takes into account all the peculiarities of the fluid flow. If such an experiment is performed, it is possible to fit the experimental points by means of $T_{w0}(y)$ and evaluate the derivatives dT_{w0}/dy and d^2T_{w0}/dy^2 at $y = s_0$ in Equation (15) and dispersion relation (19). We use below the experimental data [35] to find the temperature distribution $T_{w0}(y)$.

3. Results and Discussions

The migration velocity $c(k^+)$ from (18) can be rewritten in dimensionless form as

$$c^+(k^+) = \frac{\rho_i Lc}{h_0(T_\infty - T_f)} = c_1(k^+) + c_2(k^+),$$
$$c_1(k^+) = \frac{f(k^+)\sin[\phi(k^+)]}{k^+}, \; c_2(k^+) = \frac{k_w g_w(k^+)\sin[\psi(k^+)]}{k^+ h_0(T_\infty - T_f)}. \tag{21}$$

To calculate the migration velocity and dispersion relation, we first determined s_0 from the stationary Equation (15). As a result, the thickness of ice layer $s_0 = 19$ mm at $T_{wall} = -14.79$ °C, which is in full agreement with the experimental data [35]. Then, using s_0, we illustrate the dimensionless migration velocity $c^+(k^+)$ in Figure 3 for experimentally known range of wavenumbers $0.00075 \lesssim k^+ \lesssim 0.003$ [35]. The product $g_w(k^+)\sin[\psi(k^+)]$ defining the coefficient $c_2(k^+)$ was fitted by the function $150c_1(10k^+)k^+ - 0.3$. As is easily seen, the migration rate increases with increasing the wavenumber of perturbations.

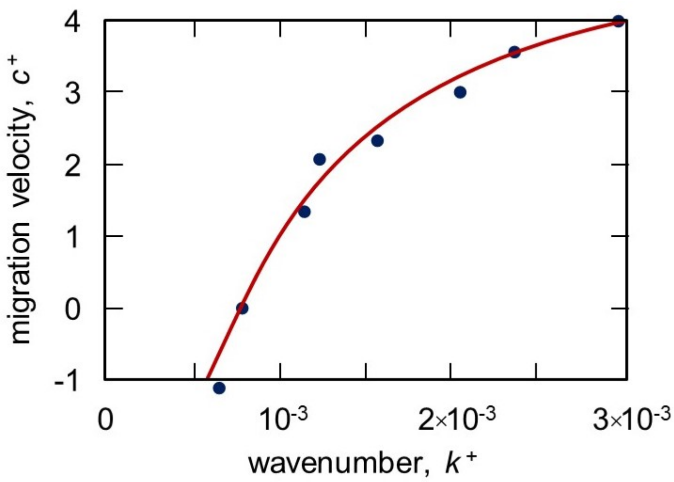

Figure 3. Dimensionless migration velocity of the wave c^+ versus dimensionless wavenumber k^+. Physical parameters used in calculations are [28,35,43]: $\rho_w = 999.8$ kg m^{-3}, $\rho_i = 1000$ kg m^{-3}, $c_w = 4.21 \times 10^3$ J kg^{-1} °C^{-1}, $k_w = 0.556$ J s^{-1} m^{-1} °C^{-1}, $k_i = 2.16$ J s^{-1} m^{-1} °C^{-1}, $L = 3.33 \times 10^5$ J kg^{-1}, $\nu_w = 1.792 \times 10^{-6}$ m^2 s^{-1}, $u_* = 0.05$ m s^{-1}, $\alpha_h = 0.0095$, $T_{wall} = -14.8$ °C, $T_\infty = 0.85$ °C.

The dispersion relation (19) is shown in Figure 4 for various temperatures T_{wall} at the cooled wall $y = 0$. Namely, the process is stable for low temperature $T_{wall} = -11.5$ °C illustrated by the solid curve (amplification rate α is negative at all wavenumbers). In other words, a groove initially made on the ice surface disappears with time and does not lead to the formation of a wavy water–ice surface. However, the amplification rate of perturbations grows with decreasing the wall temperature. The dashed and dash-dotted curves cross the axis $\alpha = 0$ and partially lie in the instability region (Figure 4). Such a behavior is very similar to the classical Mullins–Sekerka theory of morphological instability of a planar solidification front (see their Figure 1 in [18]). Note that the instability region (when a wavy water–ice surface is formed) increases with decreasing the temperature at the cooled wall. Figure 4 also demonstrates that the maximum of amplification rate ($\partial\alpha/\partial k^+ = 0$) approximately corresponds to the wavenumber $k_m^+ = 1.5 \times 10^{-3}$. In the case of instability ($\alpha > 0$), such a wavenumber (perturbation with the corresponding wavelength $\lambda_m = 2\pi\nu_w/(u_* k_m^+)$) leads to the development of morphological perturbations. Figure 5 shows that the experimental data of instability onset confirms this conclusion (instability occurs at a wavenumber lying close to the value of k_m^+). Moreover, Figure 5 demonstrates that the Reynolds number Re_δ does not substantially influence the origination/development of morphological instability.

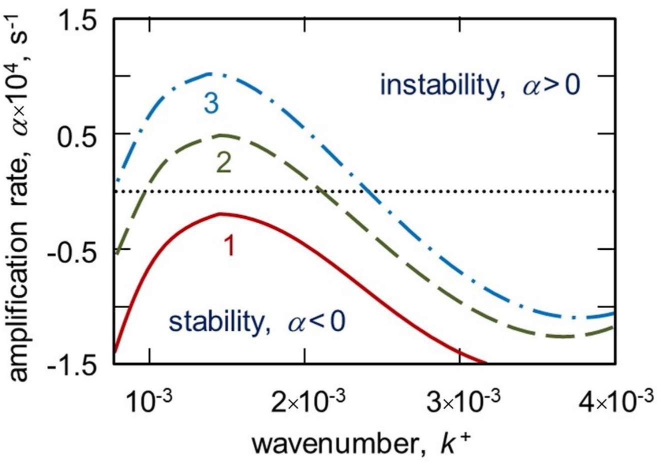

Figure 4. Amplification rate of morphological perturbations α versus dimensionless wavenumber k^+. Physical parameters correspond to Figure 3 and (1) $T_{wall} = -11.5$ °C, $s_0 = 15$ mm (solid line), (2) $T_{wall} = -14.79$ °C, $s_0 = 19$ mm (dashed line), (3) $T_{wall} = -19.9$ °C, $s_0 = 25$ mm (dash-dotted line). The horizontal dotted line $\alpha = 0$ divides the stability ($\alpha < 0$) and instability ($\alpha > 0$) domains. The phase shift is chosen so that $\cos\psi = \sin\psi$.

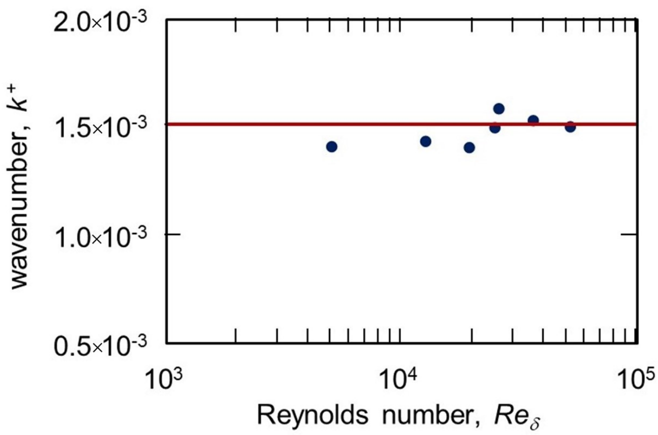

Figure 5. Dimensionless wavenumber of ice-surface waves corresponding to onset of morphological perturbations (wavy pattern formation) as a function of Reynolds number $Re_\delta = u_*\delta/\nu_w$ based on the boundary-layer thickness δ. Experiments [35] and theory are shown by symbols and solid line, respectively. Physical parameters correspond to Figure 3.

It should be noted that the present analytical model and perturbation theory do not work for a larger scale and turbulent flow. For example, taking into account the turbulent flow, when fluid particles can undergo large pulsations, the smallness of temperature perturbations near the interfacial boundary is not fulfilled. In addition, the ice surface must be smooth enough to avoid creating complex circulation currents that result in fluid mixing. Another important requirement is that the deviations of the phase interface position $\eta(x,t)$ from the flat boundary $s_0(t)$ are small enough, i.e., $|\eta(x,t)| \ll s_0$. This condition can be violated for large spatial scales as well as for small crystallization times. On the other hand, the macroscopic scale of the problem in the direction of fluid flow (direction x) must be much larger than the wavelength λ in order to disregard solid boundaries at fixed x. In general, with these limitations taken into account, the theory under consideration describes the morphological stability of wavy ice patterns with allowance for the convective–conductive heat transfer mechanism at the ice–water boundary.

An important practical application of the morphological stability theory of the water–ice interfacial boundary is the question of heat transfer at the ice surface. In the case of a wavy ice surface, the heat transfer through it is considerably higher than in the case of a flat surface [44–47]. In this case, fluid flows enhance heat transfer across the interfacial boundary, contributing to an increase in the resulting heat flux by increasing its convective component. Since the salinity of water lowers its freezing temperature and highly influences the resulting heat budget [48–50], an important direction for future investigations is the morphological stability analysis of a wavy ice surface in salty water taking convective–conductive heat and mass transfer into account. Another important task extending the present theory consists in accounting for the two-phase region on the boundary of pure ice [51–56]. Such a region essentially changes heat and mass transfer in the crystallizing system and influences the process of formation and evolution of morphological perturbations due to the presence of permeability and the possibility of liquid penetration through the water–ice interface.

4. Conclusions

In summary, we study the problem of morphological instability of the liquid–solid interface leading to the formation of a wavy ice surface. Since the fluid flow near a rough surface of solid phase (ice) is not laminar, convective–conductive heat transfer is taken into account. Bearing this in mind, we formulate the mathematical model for the growth of ice layer inside the liquid from a cooled wall. Our model accounts for small deviations of the water–ice interfacial boundary from a flat surface, which may be able to grow or decay with time. To determine the conditions of stable/unstable ice growth, we construct a morphological stability theory of the water–ice surface in the case of small perturbations. Within the framework of this theory, we have determined the stationary solution corresponding to the unperturbed equations with a flat interfacial boundary, as well as the solutions describing its perturbations. These solutions allowed us to find the migration velocity of perturbations and a dispersion relation determining the amplification rate as a function of perturbation wavenumber. Numerical analysis of the dispersion relation showed that there are stability and instability regions depending on the wavenumber of morphological perturbations and the temperature of a cold wall. As this takes place, the maximum value of the amplification rate is not essentially dependent of the wavenumber and is highly dependent of the temperature of a cold wall. This agrees with experimental data for ice-surface waves corresponding to the instability onset. Let us especially emphasize in conclusion that a nonlinear morphological stability analysis of the problem under consideration should be carried out to define the perturbation amplitudes of temperature and ice thickness. Such a theory representing a challenging task for future studies requires expanding the sought functions in Taylor series up to the cubic terms in the supercriticality parameter.

Author Contributions: Conceptualization, D.V.A. and E.V.M.; methodology, D.V.A.; software, D.V.A., E.V.M. and A.D.P.; validation, D.V.A., E.V.M. and A.D.P.; formal analysis, D.V.A., E.V.M. and A.D.P.; investigation, D.V.A., E.V.M. and A.D.P.; resources, D.V.A. and E.V.M.; writing—original draft preparation, D.V.A., E.V.M. and A.D.P.; writing—review and editing, D.V.A., E.V.M. and A.D.P.; visualization, D.V.A., E.V.M. and A.D.P.; supervision, D.V.A.; project administration, D.V.A.; funding acquisition, D.V.A. All authors have read and agreed to the published version of the manuscript.

Funding: The present research work consists of theoretical and computational parts, which were supported by different financial sources. D.V.A. acknowledges the Russian Science Foundation (Project No. 23-19-00337) for the derivation of analytical expressions, their interpretation and analysis, as well as for the processing of experimental data. D.V.A. and E.V.M. are grateful to the Ministry of Science and Higher Education of the Russian Federation (project no. FEUZ-2023-0022) for numerical simulations carried out on the basis of the theory developed.

Data Availability Statement: All data generated or analyzed during this study are included in this published article.

Conflicts of Interest: The authors declare no conflicts of interest.

References

1. Li, N.; Tuo, Y.C.; Deng, Y.; Li, J.; Liang, R.F.; An, R.D. Heat transfer at ice-water interface under conditions of low flow velocities. *J. Hydrodyn.* **2016**, *28*, 603–609. [CrossRef]
2. Rafat, A.; Pour, H.K.; Spence, C.; Palmer, M.J.; MacLean, A. An analysis of ice growth and temperature dynamics in two Canadian subarctic lakes. *Cold Reg. Sci. Technol.* **2023**, *210*, 103808. [CrossRef]
3. Alexandrov, D.V.; Netreba, A.V.; Malygin, A.P. Time-dependent crystallization in magma chambers and lava lakes cooled from above: The role of convection and kinetics on nonlinear dynamics of binary systems. *Int. J. Heat Mass Trans.* **2012**, *55*, 1189–1196. [CrossRef]
4. Nizovtseva, I.G.; Starodumov, I.O.; Pavlyuk, E.V.; Ivanov, A.A. Mathematical modeling of binary compounds with the presence of a phase transition layer. *Math. Methods Appl. Sci.* **2021**, *44*, 12260–12270. [CrossRef]
5. Notz, D.; Worster, M.G. In situ measurements of the evolution of young sea ice. *J. Geophys. Res. Ocean.* **2008**, *113*, C03001. [CrossRef]
6. Stamou, A.C.; Radulovic, J.; Buick, J.M. Effect of stenosis growth on blood flow at the bifurcation of the carotid artery. *J. Comput. Sci.* **2021**, *54*, 101435. [CrossRef]
7. Alexandrov, D.V.; Galenko, P.K. Dendritic growth with the six-fold symmetry: Theoretical predictions and experimental verification. *J. Phys. Chem. Solids* **2017**, *108*, 98–103. [CrossRef]
8. Samarskii, A.A.; Vabishchevich, P.N. *Computational Heat Transfer, Volume 1, Mathematical Modelling*; John Wiley & Sons: New York, NY, USA, 1995; pp. 15–55.
9. Vabishchevich, P.N.; Mansurov, V.V.; Churbanov, A.G. Numerical simulation of crystallization from a melt with consideration of impurity redistribution. *Russ. Chem. Ind.* **1994**, *26*, 54–70.
10. Bouissou, P.; Pelcé, P. Effect of a forced flow on dendritic growth. *Phys. Rev. A* **1989**, *40*, 6673–6680. [CrossRef]
11. Galenko, P.K.; Funke, O.; Wang, J.; Herlach, D.M. Kinetics of dendritic growth under the influence of convective flow in solidification of undercooled droplets. *Mater. Sci. Eng. A* **2004**, *375–377*, 488–492. [CrossRef]
12. Ben Amar, M.; Pelcé, P. Impurity effect on dendritic growth. *Phys. Rev. A* **1989**, *39*, 4263–4269. [CrossRef]
13. Galenko, P.K.; Jou, D. Rapid solidification as non-ergodic phenomenon. *Phys. Rep.* **2019**, *818*, 1–70. [CrossRef]
14. Choi, S.K.; Kim, S.O. Treatment of turbulent heat fluxes with the elliptic-blending second-moment closure for turbulent natural convection flows. *Int. J. Heat Mass Trans.* **2008**, *51*, 2377–2388. [CrossRef]
15. Elmakies, E.; Shildkrot, O.; Kleeorin, N.; Levy, A.; Rogachevskii, I. Experimental study of turbulent thermal diffusion of particles in an inhomogeneous forced convective turbulence. *Phys. Fluids* **2023**, *35*, 095123. [CrossRef]
16. Available online: https://cfdflowengineering.com/cfd-modeling-of-turbulent-heat-transfer/ (accessed on 18 December 2023).
17. Starodumov, I.O.; Titova, E.A.; Pavlyuk, E.V.; Alexandrov, D.V. The tip of dendritic crystal in an inclined viscous flow. *Crystals* **2022**, *12*, 1590. [CrossRef]
18. Mullins, W.W.; Sekerka, R.F. Stability of a planar interface during solidification of a dilute binary alloy. *J. Appl. Phys.* **1964**, *35*, 444–451. [CrossRef]
19. Wollkind, D.J.; Segel, L.A. A nonlinear stability analysis of the freezing of a dilute binary alloy. *Phil. Trans. R. Soc. Lond. Ser. A* **1970**, *268*, 351–380. [CrossRef]
20. Buyevich, Y.A.; Mansurov, V.V.; Natalukha, I.A. Instability and unsteady processes of the bulk continuous crystallization—I. Linear stability analysis. *Chem. Eng. Sci.* **1991**, *46*, 2573–2578. [CrossRef]
21. Buyevich, Y.A.; Mansurov, V.V.; Natalukha, I.A. Instability and unsteady processes of the bulk continuous crystallization—II. Non-linear periodic regimes. *Chem. Eng. Sci.* **1991**, *46*, 2579–2588. [CrossRef]
22. Galenko, P.K.; Danilov, D.A. Linear morphological stability analysis of the solid-liquid interface in rapid solidification of a binary system. *Phys. Rev. E* **2004**, *69*, 051608. [CrossRef]
23. Makoveeva, E.V.; Ivanov, A.A.; Alexandrova, I.V.; Alexandrov, D.V. Directional crystallization with a mushy region. Part 1: Linear analysis of dynamic stability. *Eur. Phys. J. Spec. Top.* **2023**, *232*, 1119–1127. [CrossRef]
24. Makoveeva, E.V.; Ivanov, A.A.; Alexandrova, I.V.; Alexandrov, D.V. Directional crystallization with a mushy region. Part 2: Nonlinear analysis of dynamic stability. *Eur. Phys. J. Spec. Top.* **2023**, *232*, 1129–1139. [CrossRef]
25. Loitsyanskii, L.G. *Mechanics of Liquids and Gases*; Pergamon Press: Oxford, UK, 1966; pp. 71–111.
26. Kaviany, M. *Principles of Convective Heat Transfer*; Springer: New York, NY, USA, 2001; pp. 40–46.
27. Kaviany, M. *Principles of Heat Transfer in Porous Media*; Springer: New York, NY, USA, 1991; pp. 115–528.
28. Makoveeva, E.V.; Alexandrov, D.V.; Galenko, P.K. The impact of convection on morphological instability of a planar crystallization front. *Int. J. Heat Mass Trans.* **2023**, *217*, 124654. [CrossRef]
29. Hirata, T.; Gilpin, R.R.; Cheng, K.C. The steady state ice layer profile on a constant temperature plate in a forced convection flow—II. The transition and turbulent regimes. *Int. J. Heat Mass Trans.* **1979**, *22*, 1435–1443. [CrossRef]
30. Bushuk, M.; Holland, D.M.; Stanton, T.P.; Stern, A.; Gray, C. Ice scallops: A laboratory investigation of the ice–water interface. *J. Fluid Mech.* **2019**, *873*, 942–976. [CrossRef] [PubMed]
31. Feltham, D.L.; Worster, M.G.; Wettlaufer, J.S. The influence of ocean flow on newly forming sea ice. *J. Geophys. Res. Ocean.* **2002**, *107*, 3009. [CrossRef]
32. Ashton, G.D.; Kennedy, J.F. Ripples on underside of river ice covers. *J. Hydraul. Div.* **1972**, *98*, 1603–1624. [CrossRef]

33. Weigand, B.; Beer, H. A numerical and experimental study of wavy ice structure in a parallel plate channel. In *Interactive Dynamics of Convection and Solidification*; Davis, S.H., Huppert, H.E., Müller, U., Worster, M.G., Eds.; NATO ASI Series; Springer: Dordrecht, The Netherlands, 1992; Volume 219.
34. Balmforth, N.J.; Provenzale, A.; Whitehead, J.A. The language of pattern and form. In *Geomorphological Fluid Mechanics*; Balmforth, N.J., Provenzale, A., Eds.; Springer: Berlin/Heidelberg, Germany, 2001; Volume 582, pp. 3–33.
35. Gilpin, R.R.; Hirata, T.; Cheng, K.C. Wave formation and heat transfer at an ice-water interface in the presence of a turbulent flow. *J. Fluid Mech.* **1980**, *99*, 619–640. [CrossRef]
36. Luikov, A.V. *Analytical Heat Diffusion Theory*; Academic Press: New York, NY, USA, 1968; pp. 1–34.
37. Alexandrov, D.V.; Aseev, D.L.; Nizovtseva, I.G.; Huang, H.-N.; Lee, D. Nonlinear dynamics of directional solidification with a mushy layer. Analytic solutions of the problem. *Int. J. Heat Mass Trans.* **2007**, *50*, 3616–3623. [CrossRef]
38. Nayfeh, A.H. *Introduction to Perturbation Techniques*; John Wiley & Sons: New York, NY, USA, 1981; pp. 1–133.
39. Notz, D.; McPhee, M.G.; Worster, M.G.; Maykut, G.A.; Schlünzen, K.H.; Eicken, H. Impact of underwater-ice evolution on Arctic summer sea ice. *Int. J. Geophys. Res.* **2003**, *108*, 3223. [CrossRef]
40. McPhee, M.G.; Maykut, G.A.; Morison, J.H. Dynamics and thermodynamics of the ice/upper ocean system in the marginal ice zone of the Greenland sea. *Int. J. Geophys. Res.* **1987**, *92*, 7017. [CrossRef]
41. Landau, L.D.; Lifshitz, E.M. *Fluid Mechanics*; Pergamon Press: Oxford, UK, 2013; pp. 44–226.
42. Kochin, N.K.; Kibel, I.A.; Roze, N.V. *Theoretical Hydromechanics*; Interscience Publishers: New York, NY, USA, 1964; pp. 39–80.
43. Ramudu, E.; Hirsh, B.H.; Olson, R.; Gnanadesikan, A. Turbulent heat exchange between water and ice at an evolving ice-water interface. *J. Fluid Mech.* **2016**, *798*, 572–597. [CrossRef]
44. Kruse, N.; Von Rohr, P.R. Structure of turbulent heat flux in a flow over a heated wavy wall. *Int. J. Heat Mass Trans.* **2006**, *49*, 3514–3529. [CrossRef]
45. Mohammed, H.A.; Gunnasegaran, P.; Shuaib, N.H. Numerical simulation of heat transfer enhancement in wavy microchannel heat sink. *Int. J. Heat Mass Trans.* **2011**, *38*, 63–68. [CrossRef]
46. Zhang, L.; Wang, W.; Qu, P.; Yao, X.; Song, J.; Wang, S.; Zhang, H. Study of the enhanced heat transfer characteristics of wavy-walled tube heat exchangers under pulsating flow fields. *Phys. Fluids* **2023**, *35*, 115128. [CrossRef]
47. Huang, H.; Sun, T.; Zhang, G.; Liu, M.; Zhou, B. The effects of rough surfaces on heat transfer and flow structures for turbulent round jet impingement. *Int. J. Therm. Sci.* **2021**, *166*, 106982. [CrossRef]
48. Rudels, B.; Friedrich, H.J.; Hainbucher, D.; Lohmann, G. On the parameterisation of oceanic sensible heat loss to the atmosphere and to ice in an ice-covered mixed layer in winter. *Deep Sea Res. Part Top. Stud. Oceanogr.* **1999**, *46*, 1385–1425. [CrossRef]
49. Zika, J.D.; Skliris, N.; Blaker, A.T.; Marsh, R.; Nurser, A.G.; Josey, S.A. Improved estimates of water cycle change from ocean salinity: The key role of ocean warming. *Environ. Res. Lett* **2018**, *13*, 074036. [CrossRef]
50. Van den Berk, J.; Drijfhout, S.S.; Hazeleger, W. Atlantic salinity budget in response to Northern and Southern Hemisphere ice sheet discharge. *Clim. Dyn.* **2019**, *52*, 5249–5267. [CrossRef]
51. Wettlaufer, J.S.; Worster, M.G.; Huppert, H.E. Natural convection during solidification of an alloy from above with application to the evolution of sea ice. *J. Fluid Mech.* **1997**, 344, 291–316. [CrossRef]
52. Feltham, D.L.; Untersteiner, N.; Wettlaufer, J.S.; Worster, M.G Sea ice is a mushy layer. *Geophys. Res. Lett.* **2006**, *33*, L14501. [CrossRef]
53. Alexandrov, D.V.; Ivanov, A.A. The Stefan problem of solidification of ternary systems in the presence of moving phase transition regions. *J. Exper. Theor. Phys.* **2009**, *108*, 821–829. [CrossRef]
54. Makoveeva, E.V. Steady-state crystallization with a mushy layer: A test of theory with experiments. *Eur. Phys. J. Spec. Top.* **2023**, *232*, 1165–1169. [CrossRef]
55. Toropova, L.V.; Aseev, D.L.; Osipov, S.I.; Ivanov, A.A. Mathematical modeling of bulk and directional crystallization with the moving phase transition layer. *Math. Methods Appl. Sci.* **2022**, *45*, 8011–8021. [CrossRef]
56. Toropova, L.V. Shape functions for dendrite tips of SCN and Si. *Eur. Phys. J. Spec. Top.* **2022**, *231*, 1129–1133. [CrossRef]